https://dx.doi.org/10.1016/j.jcsr.2022.107386

Experimental performance of single blind-bolted CFST column connection under predominant shear loading

Partha Pratim Debnath and Tak-Ming Chan*

Department of Civil & Environmental Engineering
The Hong Kong Polytechnic University, Kowloon, Hong Kong SAR, China
tak-ming.chan@polyu.edu.hk

Abstract

This paper presents experimental findings of ten full-scale blind-bolted concrete filled steel tubular (CFST) connection tests under predominant shear loading. Previous works show that, the performance of blind-bolts with extended shank and headed nut performed significantly well under tensile loads, but research on such connections under shear loading is at scarce. In this testing programme, the performance of individual blind-bolted CFST column connection is assessed where various parameters including presence of infill concrete, bolt embedment length, tube wall thickness and concrete strength are considered. Material tests for all the elements in the connection assembly have also been conducted. The study is accompanied by assessment of international codes. It is observed that, with higher bolt embedment length, the concrete contribution can be enhanced up to 58% of the total load applied, where the load is transmitted to the concrete core by bearing, and the tube wall yielding could also be delayed. Test results also shows that, ultimate capacity of the bolts can be achieved with CFST connections under shear load. For all the connections, the failure mode was consistent to shear fracture of bolt. At the end, a modified prediction equation for blind-bolt shear resistance is proposed. The test results presented in the investigation provides scientific data for further numerical investigations and can also provide insights towards load-introduction mechanism in bolted CFST column connections.

Keywords:

Blind-bolts, shear load, concrete filled steel tubes, extended hollo-bolts, bolted connection

1. Introduction

The use of steel-concrete composite structures is widely popular in the construction industry for decades due to several advantages offered by the combined contribution of steel and concrete. One of the composite structural elements is the concrete filled steel tube (CFST) column, whose performance in high compressive strength, better ductility, and fire resistance is evident from existing research [1-3]. Though the composite action of CFST column under axial loading is well established, but in a building the load is transferred from the floors to the column via the beam by connections, and therefore it is important to study the connection between beam and the CFST column. In this research the composite action is referred to the combined action of steel tube and concrete infill of the CFST column. Connections can be established between an open-section beam and a closed-section column, like hollow or CFST, with the help of welding or bolting. For bolting, the blind-bolts have gained wide popularity as they are specially designed to fabricate such connections where there is a lack of access inside the column tube. A typical steel-beam to CFST column connection with blind-bolts is shown in Fig.1. The blind-bolts that are currently being used in experimental research includes Ajax Australia blind-bolts [4], Lindapter hollo-bolts [5] and the slip-critical blind-bolt [6]. With the help of blind-bolts, though easy and faster joint fabrication is achieved, but the use of this technology is limited to pinned and non-moment resisting frames.

Therefore, these blind-bolts have received several modifications for tensile strength enhancement of the steel-beam to CFST column connections. The Ajax Australia blind-bolt was modified to headed anchored blind-bolts [7] and the Lindapter Hollo-bolt was modified to extended hollo-bolt [8], where the shank of the bolt has been extended with a headed nut which will provide anchorage in to the infill concrete core of the CFST column. It was observed that, due to the mechanical anchorage provided by the headed nut, the connection strength and

53 stiffness have improved significantly [7, 9]. The tensile behaviour of group of Ajax anchored
54 blind-bolts with CFST columns were studied and it was observed that the anchored blind-bolts
55 can reach the ultimate capacity of equivalent groups of standard bolts [10]. A further
56 modification of the Ajax anchored blind-bolt was made with double-headed anchorage, and the
57 Linadpater extended hollo-bolt was modified with double sleeves and observed improved
58 stiffness [11, 12]. Thus, since past few years research is being conducted to develop moment-
59 resisting frames that can combine both the benefits of composite action of CFST column and
60 the blind-bolting technology, especially with the headed anchored blind-bolt or the extended
61 hollo-bolt. Laboratory experiments to investigate the cyclic characteristics of steel-beam to
62 CFST column joints with extended hollo-bolts were conducted [13, 14]. Primarily, it was
63 observed that connections with the modified hollo-bolts high energy dissipation and higher
64 ductility can be achieved, which can be used for design of moment-resisting frames for
65 buildings in seismically active areas. The low moment-rotation stiffness displayed by
66 connections with standard hollo-bolt due to column face bending could also be improved. The
67 standard hollo-bolt and the extended hollo-bolt with headed nut is shown in Fig. 2.

68 To develop the fundamental understanding of extended hollo-bolts with the CFST column,
69 experimental, numerical, and analytical investigations were conducted based on tensile pull-
70 out tests [9, 15-17], and various failure modes including the combined failure mode have been
71 reported. The combined failure mode is referred to the failure of two or more components in
72 the connection assembly under tensile loading. Though the findings are found to be
73 encouraging in developing moment-resisting frames with extended hollo-bolts, most of these
74 investigations are conducted under direct tensile pull-out tests. Now that in a moment-resisting
75 frame, a bolted connection will be subjected to shear and bending forces, where bending can
76 be transformed to a couple of tensile force and compressive force. As a result of which, the
77 bolts will experience combined tension and shearing forces. To understand the combination of

78 tension and shearing forces on the bolts, it is imperative to realise the behaviour of the
79 connections in pure shear loading scenario. As reported in the previous findings [15, 16] that
80 the extended hollo-bolted CFST connections under tensile loading performed significantly well
81 in combined failure mode, in the next step it would be important to understand the influence of
82 the extended hollo-bolt under shear loading. As the extended shank of the hollo-bolt is
83 embedded into the concrete core, partial shear loading could possibly be transmitted to the
84 concrete core by bolt shank bearing mechanism and thereby enhancing the composite action of
85 CFST column under such loads. It also requires further investigation to effectively use the bolt
86 strength in such connections.

87 In the literature, only a few reports are found that involved the investigation of hollo-bolted
88 connections under shear loading. The behaviour of hollo-bolted angle and channel connections
89 with tubular columns under shear loads were investigated by Liu et al. [18], and reported that
90 the connection stiffness and capacity are influenced by bolt gauge distance and angle thickness.
91 The angle connections also displayed higher ductility with hollo-bolts due to the presence of
92 expandable sleeve. Another investigation on hollo-bolted connections was conducted by
93 Pitrakkos et al. [19], where standard and extended hollo-bolted connection was made with re-
94 usable steel box assembly filled with concrete, and tested under combined tension and shear
95 loading. The connections were tested under different angles of combined loading and observed
96 that the shear plane influences the connection strength, and the highest bolt ultimate strength
97 was achieved at the loading angle of 30˚. From these studies it is also inferred that independent
98 investigations on direct shear loading of hollo-bolted CFST column connections are scarce.

99 In this research, apart from understanding the pure shear behaviour of extended hollo-bolted
100 CFST column connections, there were also some limitations in the existing research [19] that
101 are addressed in this paper. In the existing investigation, the limitations can be briefly stated
102 as: the influence of bolt embedment length was not included; for the setup for the pure shear

test, the applied force was in lateral direction of the column, whereas, in a realistic situation, the shear load application along the longitudinal direction of the column would be more appropriate to observe the influence of extended hollo-bolts on concrete infill, and; in the re-usable steel box used, both the clamping plate and top plate were rigid, and therefore the influence of the tube wall thickness was ignored, and this may resemble an individual blind-bolt shear test instead of a CFST column connection shear test. Therefore, the current experimental investigation will examine the behaviour of hollo-bolted CFST column connections under predominant shear loading along with overcoming the existing experimental limitations. To understand the behaviour of extended hollo-bolted CFST column connection, in this stage of experimental investigation, a single bolt is considered in the connection assembly, which will form the basis for conducting experiments with group bolts in future studies. This current research will also be able provide some directions towards understanding of load-introduction mechanism in CFST columns with extended hollo-bolted connections, as in the current codes the observations are based on welded connections of open-beam to CFST columns.

2. Experimental testing programme

2.1 Design and construction of specimens

A total of ten full-scale blind-bolted hollow and CFST column connection specimens were prepared. The column specimens had a 4 mm thick plate welded at the bottom end to arrest any leakage of water from fresh concrete at the casting stage. Provisions for single blind-bolted connections were made at the two opposite faces of the square column specimens. This was done so that the load application can be made uniformly without any overturning of the column specimen. The length of all the specimens were 650 mm, and the connections were fabricated at mid-height position of the column, which gave enough length above and below the connection to overcome the influence of end conditions. The hollo-bolted connections were

fabricated via a rigid plate of 40 mm thickness, on which the shear loading was applied. The rigid plate was also considered so that the influence of beam end-plate thickness usually present in a beam-column connection is avoided, and the failure can be obtained in other components of the connection.

The rigid plate and the bolts were assembled to fabricate the connections on two sides of the column tube. To fix the hollo-bolts, an electric wrench was employed, and later, a handheld torque wrench was used to measure the applied torque. A torque of 300 Nm was applied, which was recommended by the hollo-bolt manufacturer. This value can also be computed as per EN 1993-1-8 [20], where bolt preload is computed by 0.7 times bolt ultimate tensile strength and bolt tensile stress area. The torque value was determined as per EN 1090-2 [21] by the product of bolt preload, factor K_m (0.2 for zinc plated bolts) and bolt diameter.

Strain gauges at desired locations were fixed previously, and necessary coating was applied for protection from water present in concrete. The concrete was poured and well compacted with the help of vibrator. After concrete casting, cling film was used to wrap the top end of the column to simulate the curing conditions of infilled concrete. Cylinders were prepared for all the batches of concrete and were also wrapped with cling film for similar curing conditions as specimens and were stored beside the specimens for same curing environment.

The specimens prepared for this experimental investigation included variation of several parameters, including steel tube wall thickness, presence of infill concrete, concrete grade, standard hollo-bolt, and different embedment length of extended hollo-bolt. In this programme, only M20 bolts of property class 8.8 were considered. The length of the bolt inside the tube specimen is considered as the bolt embedment length. The standard hollo-bolt had an embedment length of 65 mm, and there is no headed nut attached due to limited shank length. For the extended hollo-bolts, an embedment length of 92 mm and 107 mm were provisioned,

and attached with headed nut, which typically would provide the anchorage into the concrete core under tensile loading as mentioned in the introduction. Fig. 3 depicts the specimen configurations with bolted connections, as viewed from the top of the column tubes before concrete filling. The specimen references used in this paper are expressed as A-E*x*-C*y*-T*z*, where A refers to experimental series, E refers to bolt embedment length in mm, C refers to concrete grade in MPa, and T denotes steel tube wall thickness in mm. In this series, there are three repeated specimens that were adopted to confirm the test results and are represented as R at the end of the nomenclature, denoting repeat specimen. The summary of the tested specimens with geometric details are presented in Table 1. The geometric measurements of the hollo-bolts and other detailed information of the specimens are presented in Table 2.

2.2 Experimental set up

The experimental set up was built up with several steel assemblies to be seated in MTS 815 Rock Mechanic testing system having a capacity of 460 tons. The MTS system has circular crossheads in both upper and bottom sides, where the bottom crosshead has a travel of ± 50 mm. For mounting the specimen, a support base plate of 50 mm thickness was placed on the bottom crosshead. Four position bars were placed on the steel support plate, through which threaded screws were used to “fix” the specimen at the base. An inverted U-frame, to be referred as reaction frame here onwards, was fabricated with high strength steel to apply the load to the bolted connections and is designed to remain elastic under the applied load. The load applied via the reaction frame resembles the load from the beam to the connection in a typical site situation. The reaction frame has three parts, an upper part of dimension 360 × 250 × 80 mm and two legs having dimension 315 × 270 × 50 mm, all of which can be assembled with bolts. The legs are placed on the rigid stub plates of the connection assembly, through which the shear load was applied. Two balance bars were also bolted at the front and rear sides of the reaction frame, to keep a check on the uniform positioning of the loading legs at the

177 initial stage of test. It is worth mentioning that the position of the reaction frame was such that,
178 there is a gap of 5 mm between the steel tube specimen and load frame legs on both the sides,
179 so that there is no load transfer via contact between the legs and the column surface. A
180 minimum gap of 5 mm was also necessary so that the reaction frame can be placed with ease
181 over the square specimens. And thus, a predominant shear loading setup for the blind-bolted
182 tube connection specimens was built. A three-dimensional sketch of the setup is presented in
183 Fig. 4. A compression platen was placed on the upper part of the reaction frame to touch the
184 load cell that is attached to the fixed crosshead of the MTS machine. As the moveable crosshead
185 of the machine travels upwards, the load is transferred to the connections via the inverted U-
186 frame, uniformly on both the sides. A loading rate of 0.3 mm/min was adopted for all the tests
187 which is appropriate to capture the static load-displacement behaviour of the specimens. The
188 actual experimental setup using the MTS testing system and close view of the bolted
189 connection region is presented in Fig. 5 (a) and (b), respectively.

190 *2.3 Instrumentation*

191 To accurately capture the load-displacement behaviour and strain distribution in the connection
192 region, several linear variable differential transducers (LVDTs) and strain gauges were
193 employed. The LVDTs (L1 and L2) and were placed on two sides of the support plate, that
194 measured the travel along the loading direction. Another LVDT (L3) was attached to the right-
195 side connection rigid plate, to keep a check of any displacement in the reaction frame, which
196 is supposed to be devoid of any movement. In the results, the average of L1 and L2 was
197 considered to represent the load-displacement behaviour of the specimens. To measure the
198 strain distribution in the steel tube, in proximity to the connection region, two tube strain gauges
199 (TSG1 and TSG2) were attached in the inside region of the tube wall. These strain gauges were
200 positioned in the longitudinal direction of the applied load and located in bottom side of the
201 bolt holes. Strain gauges were not attached in the outer side of the tube as they could potentially

202 be damaged by the rigid plates undergoing high clamping forces while fabrication of the
203 connection. To monitor the strain developed in the extended shank of the hollo-bolt and in the
204 adjoining concrete region two strain gauges were attached in each bolt (BSG1 ~ BSG4), near
205 the bolt headed nut. The connections under shear loading, the bolt shanks are expected to
206 undergo bending stresses, where the upper shank region experiencing tension forces, and the
207 lower shank region experiencing compressive forces, which will possibly be captured by the
208 BSG strain gauges. All the strain gauges (TSGs and BSGs) were applied with water proofing
209 coating with SB tape to protect from the infill fresh concrete. It requires to be mentioned that,
210 for the specimens with standard hollo-bolts, no bolt strain gauges could be attached due to
211 limited shank length. To keep a check on any rotation of the hollo-bolted connections,
212 inclinometers (IN1 and IN2) were attached to the rigid plates on both sides. The positioning of
213 the LVDTs, strain gauges and the inclinometers is presented in Fig. 6. The inside view of the
214 hollow steel tube, with strain gauges attached to steel surface and bolt shank is presented in
215 Fig. 7.

216 *2.4 Material tests*

217 As the connection assembly consists of steel tube, concrete, and the blind-bolt components, it
218 is therefore pertinent to conduct material tests of these elements. For the steel tubes, as two
219 different thickness of 6.3 mm and 8 mm were considered in this testing programme, flat dog-
220 bone shaped coupons were extracted from these steel tubes and were designed as per ISO 6892-
221 1:2019(EN) [22]. For each batch, three coupons were tested at a loading rate of 0.3 mm/min
222 until 3% strain, a rate of 0.6 mm/min was used from 3% strain to yield strain, and beyond yield
223 strain a loading rate of 1.2 mm/min was adopted. Fig. 8 presents the test setup of flat steel
224 coupons using the Instron machine. For the M20 hollo-bolts, as three different embedment
225 lengths were used in this experimental programme, they were supplied from three different
226 batches. The length of the bolts were 120 mm, 150 mm, and 165 mm, which had embedment

lengths of 65 mm, 92 mm, and 107 mm, respectively, inside the tube (refer Fig. 3). As they were from different batches, three circular coupons of each bolt length were considered for the material testing. For the circular coupons, a loading rate of 0.02 mm/min was adopted until strain of 1% is reached, 0.2 mm/min loading rate was used from 1% strain to 7% strain, and beyond 7% strain a loading rate of 0.5mm/min was used. For all the steel material coupon testing Instron UTM machine was used. Apart from the video extensometer, strain gauges were attached to all flat steel and circular bolt coupons to accurately measure the elastic modulus. For the hollo-bolt sleeve, through which the shear plane passes, were also tested for its mechanical properties using Rockwell hardness testing machine. These hardness test values were later converted to material strength values. Referenced images for tested flat coupons and circular bolt coupons are presented in Fig. 9 (a) and (b), respectively. The stress-strain plots for 6.3 mm flat steel coupons and 120 mm circular bolt coupons are presented in Fig. 10 and Fig. 11, respectively. The measure material properties of steel tubes, bolt shank and bolt sleeve are provided here in Table 3. Two concrete grades C40 and C80 were used in this experiment, for which cylinders of size 100 mm diameter and 200 mm length were casted. They were tested for both compressive and split tensile strength. The compressive stress-strain plot obtained with the help of strain gauges attached to the concrete cylinders are presented in Fig. 12. Concrete grade C40 was commercially supplied, whereas C80 was manufactured in the laboratory. The concrete mix ratios and measured material properties are provided in Table 4.

3. Connection behaviour and failure modes

The specimen for standard hollo-bolted connection with hollow steel tube was tested to study the influence of concrete infill under predominant shear loading. As observed in Fig. 13 for the tested specimen A-E65-C0-T6.3, the bolts have undergone bending deformation, with fracture in the leaves of the sleeve. The location of sleeve fracture is at the region where the sleeves

open up upon tightening as shown in Fig. 13 (a). As the shear loading is applied, the load is transferred to the steel tube wall, and this generates a deformation in the lower half-circle of the bolt hole, as shown in Fig. 13 (b). Upon removal of the standard hollo-bolts from the specimen, it can be observed that the sleeve has undergone full deformation and touched the conical nut and bolt shank. Similarly, the sleeve surface abrasion and fractured sleeves can also be observed from the Fig. 14. It is also to be noted that, apart from the threaded shank region, the shear plane also passes though the slotted sleeve region of the bolt assembly, and sleeves are the first load bearing element under the shear loading.

The specimen A-E65-C40-T6.3 having standard hollo-bolt and infill concrete, had shear failure of the bolt, where both the sleeve and the shank have undergone total fracture under the sustained loading. The tested specimen in presented in Fig. 15 (a), where the shear fracture plane is shown. Upon inspection of the internal concrete damage by cutting the steel tube skin in the connection region, it was observed that minor concrete cracks were developed around the bolt. The deformation in the steel tube was primarily bulging in the tube interior wall, which is marked in white as shown in Fig. 15 (b). As shown in Fig. 15 (c), under the effect of shear loading, the sleeves were compressed in one side, whereas the other side remained uncompressed, and thus forming a gap between the bolt and the rigid plate.

As the bolt embedment length was increased from 65 to 92 mm with a headed nut, the specimen A-E92-C40-T6.3 also failed in bolt shearing. The original and after test position of the stub can be seen in Fig. 16 (a), and for this specimen the test was stopped as the load dropped sharply and did not continue to full shear fracture of the bolt. Similarly, for the specimen A-E107-C40-T6.3, the connection failed in bolt shear, and the left and right-side views of the specimen is shown in Fig. 16 (b) and (c), respectively. It is to be mentioned that, both the sides of the specimen did not fracture fully at the same time possibly due to not so perfect positioning of the bolt through the column tube holes. Upon removal of the concrete skin from the specimen

277 A-E107-C40-T6.3, it is observed that there are no visible concrete cracks, but the bulged
278 deformation of the tube interior wall is evident as shown in Fig. 17 (a). The part of the fractured
279 hollo-bolt that remined with the stub plate is shown in Fig. 17 (b) and (c), which clearly
280 represents that the shear plane passes through the slotted region of the sleeve and the threaded
281 shank. As presented in Fig. 17 (c), the non-perfect plain surface of the bolt shank could possibly
282 be because of a tension component that might arise due to small moment generated from the 5
283 mm gap between reaction frame legs and the specimen.
284 The failure mode of the repeat specimens A-E65-C40-T6.3-R and A-E107-C40-T6.3-R is also
285 dominated by bolt fracture, which confirms the reliability of the tests. With an enhanced tube
286 thickness of 8 mm for the specimen E92-C40-T8, no significant bearing failure in concrete or
287 steel tube was observed, and the failure was observed by bolt shear fracture. The position of
288 the fractured extended hollo-bolts attached to the CFST part and rigid plate part after the test
289 for the specimens A-E107-C40-T6.3-R and A-E92-C40-T8 are shown in Fig. 18. The fractured
290 bolt part attached to the CFST has a gap formation in the upper region, whereas for the bot part
291 attached to the rigid plate the gap formation is in the lower region, which is a typical shear
292 failure pattern. The specimens A-E107-C80-T6.3 and A-E107-C80-T6.3-R fabricated with
293 high strength concrete of C80 were tested to investigate the influence of concrete strength in
294 the failure pattern of the bolted connections. As observed from Fig. 19, the connection failed
295 by shear fracture of the bolts, and there has been no visible cracks in the concrete and limited
296 bulging of the inner surface of the steel tube wall. The fractured bolt attached to the rigid plate
297 and the surface of the bolt shank are also presented in Fig 19.
298 Thus, from the above observations, it is noted that for hollow steel tube connections the failure
299 is governed by total deformation of sleeve and bending of the bolt shank. Whereas, for all the
300 bolted CFST connection specimens, the failure was governed by total shear fracture of the bolt
301 sleeve and shank, irrespective of the tube wall thickness, bolt embedment length and concrete

graded strength. Under this predominant shear loading, no bearing failure was observed, and all the failure modes were by combined sleeve and shank fracture along the direction of the shear plane.

4. Results and discussion

4.1 Load-displacement

In this section, the shear load versus connection displacement behaviour is discussed, and the summary of the test results is presented in Table 5. The load values presented here refers to force per bolt in the tested specimens. The bolted connection with hollow tube (A-E65-C0-T6.3), the entire load was transferred to the tube wall, and as a result the tube underwent significant stress. The failure was by excessive deformation of the sleeve and bending of bolt shank, the peak load achieved was 238.5 kN, with a stiffness of 58.82 kN/mm. Whereas, when the specimen was filled with concrete (A-E65-C40-T6.3), the specimen achieved a peak load of 272.5 kN and a stiffness of 105.8 kN/mm, which is about 14% improvement in strength and 80% improvement in connection stiffness, respectively, as compared to the hollow specimen. The load-displacement plot of the hollow and concrete-filled specimen is presented in Fig.20. This refers that a significant load was transferred to the concrete infill by the bolt embedment length of $3.25d_b$, and the bolt was able to achieve its full strength, where d_b is the bolt diameter. A comparison for the repeated specimen A-E65-C40-T6.3-R, and its counterpart specimen is presented in Fig. 21, where the peak load, stiffness and failure modes are in good agreement, indicating reliability of the test results. For the specimen with longer bolt embedment length of $4.6d_b$ (92 mm), achieved a peak load of 286.5 kN, and displayed a stiffness of 73 kN/mm. The comparison between the specimens A-E65-C40-T6.3 and A-E92-C40-T6.3 is presented in Fig. 22. It is to be noted that, both the specimens ultimately failed by bolt shearing, as mentioned in the previous section. Initially, it may look that higher embedment length generated a higher peak load, but it is not the case, and will be discussed in the later part of this section. The specimen with bolt embedment length of $5.35d_b$ (107 mm), A-E107-40-T6.3 achieved a peak

328 load of 245.5 kN, and the corresponding repeat specimen A-E107-C40-T6.3-R achieved a peak
329 load of 240 kN, which is a slight variation of 2.3%, and is shown in Fig. 23.
330 Similarly, by reducing the steel tube section slenderness from 39.6 to 31.25, i.e, by increasing
331 the tube thickness from 6.3 mm to 8 mm, the failure mode of the connection was still by bolt
332 shear fracture, and the peak load achieved by the specimen A-E92-C40-T8 is 293.5 kN, which
333 is just varied by 2.5% as compared to A-65-C40-T6.3 and is presented in Fig. 24. With the
334 increase in concrete strength to C80, the specimen A-E107-C80-T6.3, when compared to its
335 counterpart specimen A-E107-C40-T6.3, though the peak load was close to each other, 266.5
336 kN and 245.5 kN respectively, but the stiffness was improved by the presence of higher strength
337 concrete. The stiffness had improved by almost 18% possibly due to higher elastic modulus
338 offered by C80 grade concrete as compared to C40 grade concrete and is shown in Fig. 25. The
339 repeat specimen A-E107-C8-T6.3-R is plotted with its counterpart to check the consistency of
340 the behaviour, and is shown in Fig. 26, which confirms that the stiffness and peak load achieved
341 are in good agreement to each other.

342 Now, as far as the strength of the connections with CFST columns are concerned, irrespective
343 of the bolt embedment length of $3.25d_b$, $4.6d_b$ and $5.35d_b$, all the specimens had failed by bolt
344 shearing at the shear plane, and therefore the ultimate strength of these connections were
345 governed by the actual bolt strength. As can be referred from Table 3, the ultimate strength of
346 the bolts with shank length 150 mm (used as $4.6d_b$ embedment length) had higher mechanical
347 strength, as compared to bolts with shank length of 120 mm and 165 mm. And thus, the A-
348 E92-C40-T6.3 had higher capacity than A-E65-C40-T6.3 and A-E107-C40-T6.3, but all of
349 them had consistent failure mode, i.e, shear fracture of the bolt. It can also be stated that, with
350 bolt embedment length into the concrete core, the full capacity of the bolt could be achieved
351 along with partial load transfer to the infill concrete by bolt shank bearing. Similarly, when
352 tube the tube wall thickness was increased, there has been no change in the failure pattern

353 mode, and no prominent bearing failure was observed. Whereas, with increase in concrete
354 grade to C80, though the connection failed in bolt shear fracture, an increase in stiffness was
355 achieved possibly due to higher bearing capacity provided by the higher elastic modulus of the
356 infill concrete.

357 *4.2 Load transfer mechanism*

358 As can be observed from all the shear load versus slip curves, the connection behaviour pattern
359 can be presented in four-stages, as presented in Fig. 27. The initial behaviour up to 4 mm
360 displacement and load of 100 kN is captured for two specimens and is shown in Fig. 27 for
361 reference and discussion. As the nominal hole diameter for the M20 hollo-bolts were 35 mm,
362 and the nominal external diameter for the sleeve is 32.75 mm, a slip between the bolt and tube
363 hole was observed in almost all the specimens. Based on this experimental programme, the
364 average slip value can be computed to about 0.5 mm. Secondly, as the shear plane passes
365 through the expandable sleeve, the load is initially borne by the sleeve component and thus the
366 corresponding stiffness is offered by the sleeve. This initial stiffness is maintained up to a load
367 of about 40 kN, at which the sleeve yielding begins. After the yielding of the sleeve, it is
368 followed by post-yield hardening and gradual transfer of the load to the bolt shank starts which
369 occurs approximately at around 65 kN. At this point, the sleeve which has an internal diameter
370 of 21 mm, the contact with the bolt shank takes place, and the load begins to transfer to the
371 shank. Thus, in this research programme, the stiffness of the connection can be considered from
372 the resistance against deformation offered by the bolt shank and is measured at the linear part
373 of the load-displacement curves, referred to as k and mentioned in Table 5. The average
374 stiffness for all the CFST specimens is 101 kN/mm and a CoV of 25% can be obtained. The
375 stiffness at 70% of the ultimate connection resistance is also calculated as per Eurocode 4 [23],
376 where the average stiffness is computed to be 97 kN/mm, with a CoV of 21.6. This stiffness
377 can be referred as connector stiffness, $k_{sc,}$ as mentioned in Table 5.

4.3 Strain development

The strain developed in the steel tube, just below the bolt hole (refer to Fig.6) is presented in Fig. 28, where negative strain corresponds to compressive stresses. In the hollow steel tube specimen, the stresses are significantly higher as the load is resisted solely by tube wall bearing, and the tube yielded at a load of 55 kN and the maximum strain reached a value of around -40000 με (refer Fig. 28a). At around 135 kN, there is reversal in the strain as at this load the bolt started to bend upwards and the stresses in the lower part of the bolt hole gradually reduced. With bolted connection when infilled with concrete, the bolt embedment has been able to transfer a considerable load to the concrete core by bearing, and as a result the steel tube delayed its yielding to around 85 kN (refer Fig. 28b), and the maximum strain reached up to -12000 με. As also can be referred from Fig. 28 (c-h), as the bolt embedment length was increased, there has been a significant delay in tube wall yielding load. This signifies that a considerable shear load was transmitted to the concrete core by bolt shank bearing mechanism. This phenomenon also indicates that an enhanced composite action can be achieved with CFST columns under shear loading with the use of extended hollo-bolts, that are embedded into the concrete core.

A representative image for the strain developed in the bolt shank (BSG), is presented in Fig. 29. As the strain gauge was fixed to the bolt shank next to the headed nut, embedded into the concrete core, the measured strain can also be referred as the strain developed in that region. The part of extended bolt shank, which is embedded into the concrete, due to the applied shear load, will undergo bending. And as a result, the upper region of the shank will experience tensile stresses, while the lower region will have compressive stresses. As shown in Fig. 29, for the specimen A-E92-C40-T6.3, having a bolt embedment length of 92 mm, strain gauges BSG1 and BSG2 (fixed at 180˚ to each other) refers to the bolt strain gauges attached to the bolt in left-side connection, where the solid line represents region under compression, and the

dotted line represents region under tension. Similar is the case with BSG3 and BSG4 attached to the bolt in the right-side connection. This strain distribution signifies the transfer of shear load to the concrete infill via the bolt embedment length, and the amount of strain developed is very close to 2790 με, which is the concrete strain at peak stress (for C40 grade concrete). For the specimens having embedded bolts with attached strain gauges (BSG), the amount of concrete contribution was calculated from the bolt strain values as shown in the representative Fig. 29. The stress value was obtained from the bolt strain at the peak load, which indicates the amount of load transfer to the concrete core by bearing. This can be referred to as the concrete contribution in total shear load transfer, where a part of the load is borne by the tube wall, and the remaining by the concrete core. Specimens with bolt embedment lengths of $4.6d_b$ and $5.35d_b$ show that the concrete contribution in load transfer can be up to 58% of total applied force, indicating enhanced composite behaviour of the CFST column under the applied shear loading.

5. Assessment of design codes

As observed from the failure modes of the blind-bolted CFTS connections, all of the specimens ultimately failed by bolt shear fracture. Though the beneficial effect of infill concrete, bolt embedment length, higher concrete grade and tube wall thickness is realized, but the failure mode for the all the concrete-filled specimens were consistent. It is therefore can be stated that, under predominant shear loading, both the standard and extended single hollo-bolted CFST connections undergoes bolt shear fracture, and no prominent signs of concrete bearing failure could be observed. Now to assess the applicability of the existing design codes to predict the shear failure of the standard and extended hollo-bolted CFST connections, the equations provided by the Eurocode 3 [20], AISC-360 [24] and AS4100 [25] were selected. The expressions to determine the shear resistance for bolts, for the shear plane passing through the

threads as per the European code, North American code and Australian code are given in eq (1), (2) and (3), respectively, while the comparison with the test data is presented in Table 5.

$$F_{v,EC3} = \alpha_v f_{u,b} A_b \quad (1)$$

$$F_{v,AISC} = 0.563 f_{u,b} A_b \quad (2)$$

$$F_{v,AS} = 0.62 f_{u,b} A_{b,c} \quad (3)$$

where,

F_v is the shear resistance capacity in kN;

α_v is the co-efficient, 0.6 for bolt class 8.8;

$f_{u,b}$ is the bolt ultimate tensile strength MPa;

A_b is tensile stress area of the bolt in mm^2;

$A_{b,c}$ is core area of the bolt in mm^2

As can be seen from Table 5, all the three design approaches used in these codes provides highly conservative predictions of the hollo-bolted connection shear resistance. The primary reason for such conservative prediction is that EC3, AISC and AS formulae are not developed based on such blind-bolts and therefore does not include the capacity of the hollo-bolt expandable sleeve, through which the shear plane passes, in addition to the bolt threaded shank. Therefore, based on the current experimental test results, eq (4) is proposed which considers the strength of bolt expandable sleeve and shank for prediction of the hollo-bolt shear capacity. The co-efficient of 0.6 still fits well in the proposed equation. As seen, in Table 5, the shear resistance has a maximum deviation of 10% for the hollo-bolted CFST connection specimens when compared between the test results and the proposed strength values.

$$F_{v,Prop} = 0.6\,(f_{u,b} A_t + f_{u,sl} A_{sl}) \quad (4)$$

where,

$f_{u,sl}$ is the sleeve ultimate strength in MPa

A_{sl} is the net sleeve area in mm^2

Thus, based on the proposed equation the shear resistance for both the standard and extended hollo-bolts can be predicted with high accuracy, and similarly the design shear resistance can also be predicted with incorporation of the code based partial safety factors in the same equation. Further comparison can also be made to determine the relation between shear strength of hollo-bolts with its tensile capacity. The tensile coupon tests conducted for the bolt shank as previously presented in Table 3 can be used to compute the hollo-bolt tensile capacity, where the tensile capacity is determined by product of the ultimate tensile strength and the area of the threaded bolt shank. From comparison, it is observed that the average shear strength capacity of the hollo-bolt is approximately 1.20 times its tensile strength capacity.

6. Conclusions

This paper has presented an experimental investigation of ten full-scale hollo-bolted CFST connection under predominant shear loading. At this stage of the experimental programme, only single bolted connections with square CFST columns were considered to understand the failure modes, strength, and overall behaviour of the specimens. Several parameters like, infill concrete, bolt embedment length, concrete grade, tube wall thickness was considered to quantify the shear behaviour of the bolted connections. The research programme is also supported by material tests conducted for the steel tube, bolt, and concrete, which will help to conduct further numerical studies with a wide range of parameters and supplement the current limited test results. From this research the following conclusions can be drawn:

1. The standard hollo-bolted CFST connection displayed a significant improvement of 80% in connection stiffness, and 14% strength improvement due to the presence of concrete as

compared to the specimen without infill concrete. As the standard hollo-bolt has an embedment length of 3.25d_b, it was possible to arrest the bending of the bolt by the surrounding concrete, and thereby increasing the connection stiffness.

2. The initial stiffness of the connections is significantly less up to a load of approximately 30% of the ultimate load, as until this load the stiffness is influenced by the hollow sleeve. Upon yielding of the sleeve and transfer of load to the shank, the stiffness stabilises, and is measured at 70% of the ultimate resistance. The average stiffness for all the bolted CFST connections is computed to 97 kN/mm with a CoV of 21.6.

3. All the bolted CFST connections had a consistent failure mode of bolt shear fracture along the shear plane. The mean ultimate shear resistance for the single standard and extended hollo-bolted CFST connection can be computed to 1.2 times the bolt tensile capacity. For the connections that involved extended hollo-bolt, no prominent bearing failure of concrete was observed. For the column tube wall, bulging effect near the hole can be observed due to the compressive forces transferred from the bolt bearing on the tube.

4. The prediction equations for shear resistance of both standard and extended hollo-bolts as per the design approaches in EC3, AISC-360 and AS4100 are very conservative. Therefore, based on the test results this paper proposed an equation incorporating the expandable sleeve strength which can predict the bolt shear resistance with a maximum of 10% deviation. This predictive equation will be useful to determine the strength of hollo-bolted CFST connection subjected to shear loading.

5. Though the bolt embedment length of 3.25d_b, 4.6d_b and 5.35d_b did not alter the connection failure mode, but the extended bolt shank has been able to significantly transmit the shear load to the concrete core by bearing mechanism, which is confirmed by internal strain distribution reaching concrete strain at peak stress. Simultaneously, a reduction in stresses in steel tube

could be attained, and connection load for tube yielding was also delayed. With higher concrete grade, an increase in connection stiffness of 18% was achieved as compared with specimen having normal strength concrete.

6. The experimental results reveals that, hollo-bolted connections with CFST columns under shear loading full ultimate bolt capacity can be achieved. Also, enhanced composite behaviour of CFST columns can be realized with embedded hollo-bolts due to concrete contribution in shear load transfer.

7. Based on the shear tests and previously conducted tensile tests by the authors, further investigation under combined tension and shear loading can be carried out to generate tension-shear interaction relationship for standard and extended hollo-bolted CFST connections.

Acknowledgement

The authors sincerely acknowledge the support received from the Chinese National Engineering Research Centre for Steel Construction (Hong Kong Branch) at The Hong Kong Polytechnic University.

References:

[1] L.-H. Han, W. Li, R. Bjorhovde, Developments and advanced applications of concrete-filled steel tubular (CFST) structures: Members, Journal of Constructional Steel Research 100(C) (2014).

[2] J. Chen, T.-M. Chan, K.-F. Chung, Design of square and rectangular CFST cross-sectional capacities in compression, Journal of Constructional Steel Research 176 (2021) 106419.

[3] Z. Tao, L.-H. Han, B. Uy, X. Chen, Post-fire bond between the steel tube and concrete in concrete-filled steel tubular columns, Journal of Constructional Steel Research 67(3) (2011) 484-496.

[4] AJAX, ONESIDE Brochure B-N012 Data Sheet, (2002).

[5] Lindapter, Brochure of Hollo-Bolt by Lindapter, Bradford, UK, (2018).

[6] W. Wang, M. Li, Y. Chen, X. Jian, Cyclic behavior of endplate connections to tubular columns with novel slip-critical blind bolts, Engineering Structures 148 (2017) 949-962.

[7] H. Agheshlui, H. Goldsworthy, E. Gad, S. Fernando, Tensile behaviour of anchored blind bolts in concrete filled square hollow sections, Materials and Structures 49(4) (2016) 1511-1525.

[8] T. Pitrakkos, W. Tizani, Experimental behaviour of a novel anchored blind-bolt in tension, Engineering Structures 49 (2013) 905-919.

[9] W. Tizani, T. Pitrakkos, Performance of T-Stub to CFT Joints Using Blind Bolts with Headed Anchors, Journal of Structural Engineering 141(10) (2015) 04015001.

[10] H. Agheshlui, H. Goldsworthy, E. Gad, H. Yao, Tensile Behavior of Groups of Anchored Blind Bolts within Concrete-Filled Steel Square Hollow Sections, Journal of Structural Engineering 142(2) (2016) 04015125.

[11] Y. Oktavianus, H.M. Goldsworthy, E.F. Gad, Cyclic behaviour of individual double headed anchored blind bolts within CFST, Journal of Constructional Steel Research 133 (2017) 522-534.

[12] M.Z. Jeddi, N.H.R. Sulong, Pull-out performance of a novel anchor blind bolt (TubeBolt) for beam to concrete-filled tubular (CFT) column bolted connections, Thin-Walled Structures 124 (2018) 402-414.

[13] W. Tizani, Z.Y. Wang, I. Hajirasouliha, Hysteretic performance of a new blind bolted connection to concrete filled columns under cyclic loading: An experimental investigation, Engineering Structures 46 (2013) 535-546.

[14] W. Tizani, A. Al-Mughairi, J.S. Owen, T. Pitrakkos, Rotational stiffness of a blind-bolted connection to concrete-filled tubes using modified Hollo-bolt, Journal of Constructional Steel Research 80 (2013) 317-331.

[15] P.P. Debnath, T.-M. Chan, Tensile behaviour of headed anchored hollo-bolts in concrete filled hollow steel tube connections, Engineering Structures 234 (2021) 111982.

[16] M. Cabrera, W. Tizani, M. Mahmood, M.F. Shamsudin, Analysis of Extended Hollo-Bolt connections: Combined failure in tension, Journal of Constructional Steel Research 165 (2020) 105766.

[17] P.P. Debnath, T.-M. Chan, A comprehensive numerical approach for modelling blind-bolted CFST connections, Structures 33 (2021) 2208-2225.

[18] Y. Liu, C. Málaga-Chuquitaype, A.Y. Elghazouli, Behaviour of beam-to-tubular column angle connections under shear loads, Engineering Structures 42 (2012) 434-456.

[19] T. Pitrakkos, W. Tizani, M. Cabrera, N. Faqe Salh, Blind bolts with headed anchors under combined tension and shear, Journal of Constructional Steel Research 179 (2021) 106546.

[20] CEN, Eurocode 3 : Design of Steel Structures- Part 1-8: Design of Joints. BS EN 1993-1-8: 2005, (2005).

[21] B.S. Institution, EN 1090-2:2018 Execution of steel structures and aluminium structures, (2018).

[22] ISO, British Standards Institution 6892-1:2019(EN) Metallic materials — Tensile testing — Part 1: Method of test at room temperature, (2019).

[23] CEN, CEN 1994-1-1, Eurocode 4: Design of Composite Steel and Concrete Structures – Part 1-1: General Rules and Rules for Buildings, (2009).

[24] ANSI/AISC, ANSI/AISC 360-16. Specification for structural steel buildings, (2016).

[25] AS, AS 4100 -1998 (R2016), Steel Structures, (2016).

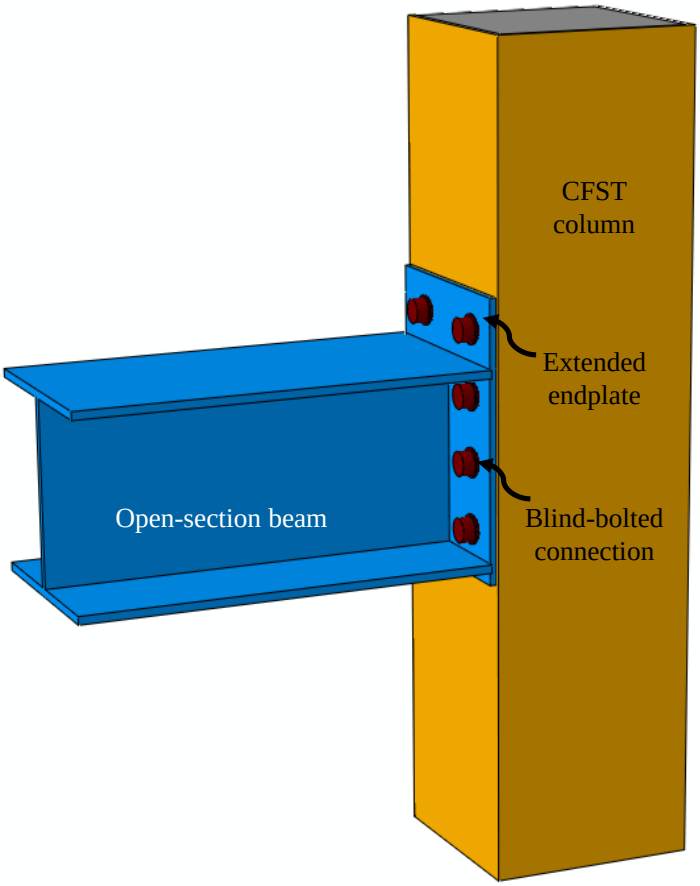

Fig. 1: Typical blind-bolted beam to CFST column connection.

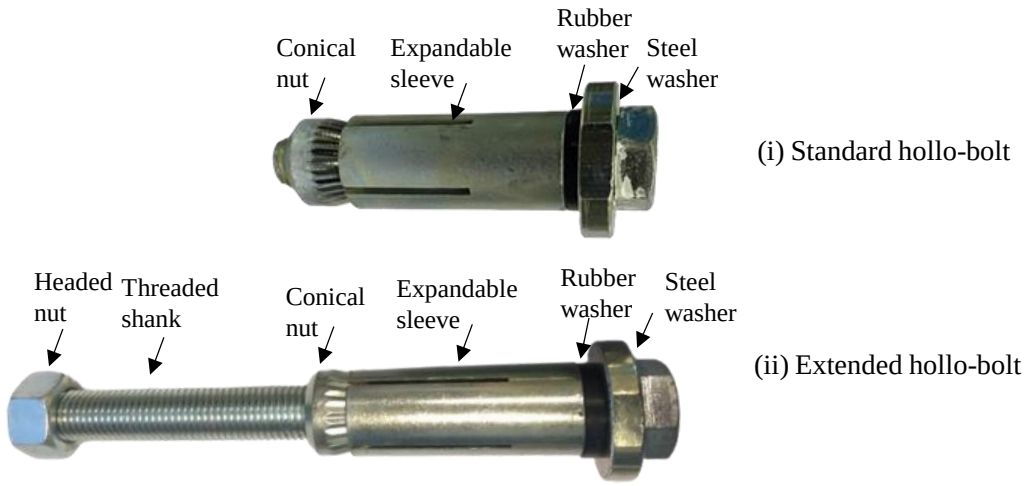

Fig. 2: The standrad hollo-bolt and extended hollo-bolt.

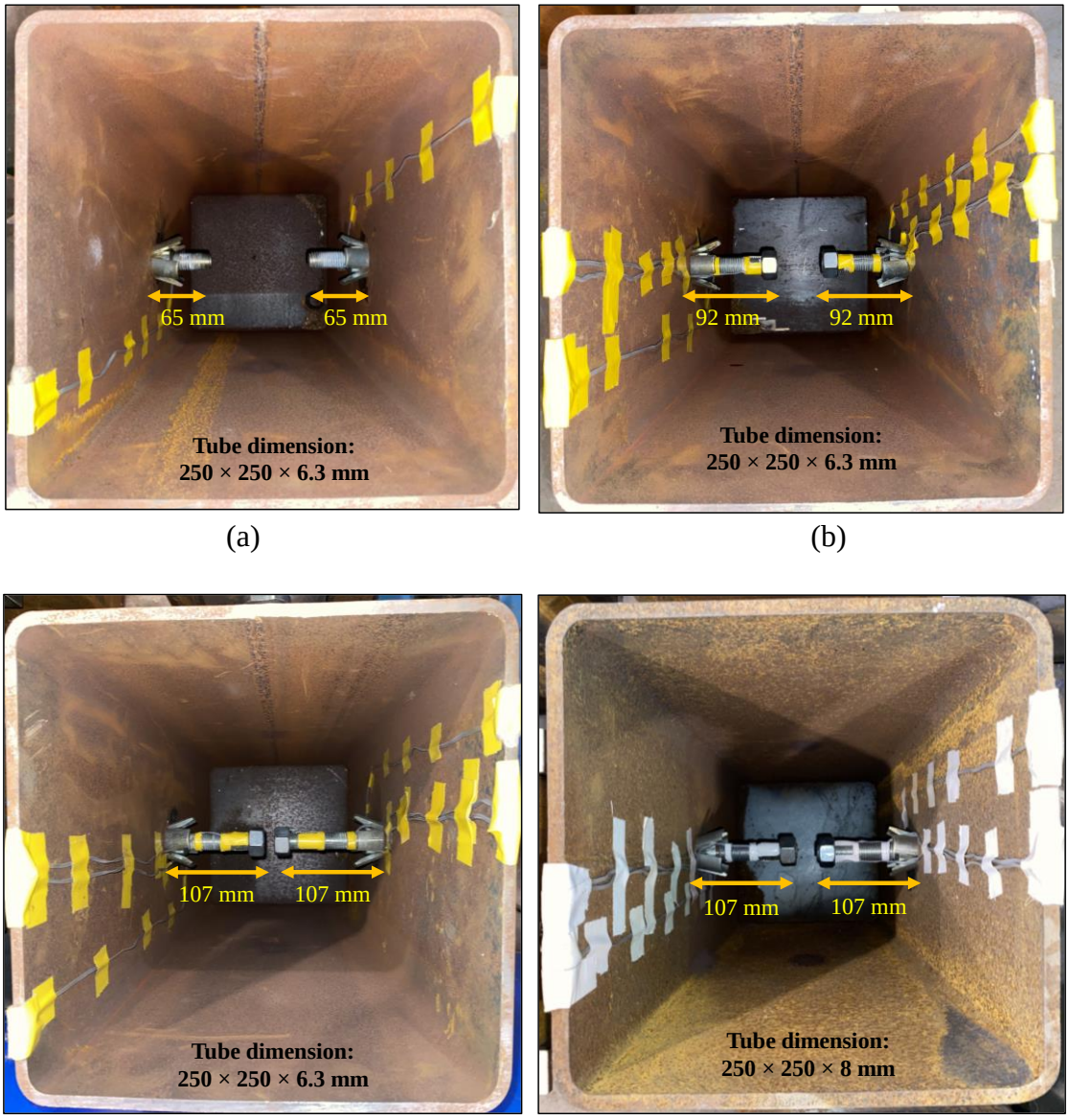

(a) (b)

(c) (d)

Fig. 3: Steel tube specimens with different bolt embedment lengths and tube cross-sections.

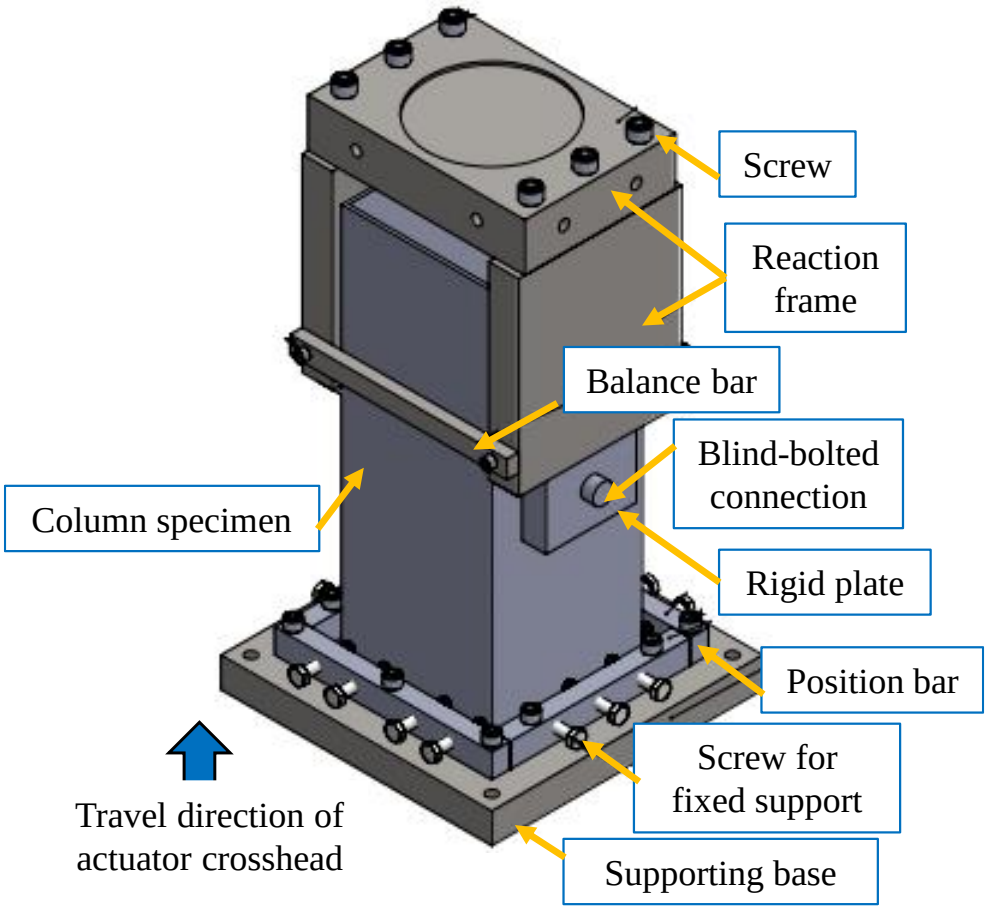

Fig. 4: Three-dimensional sketch of the experimental setup.

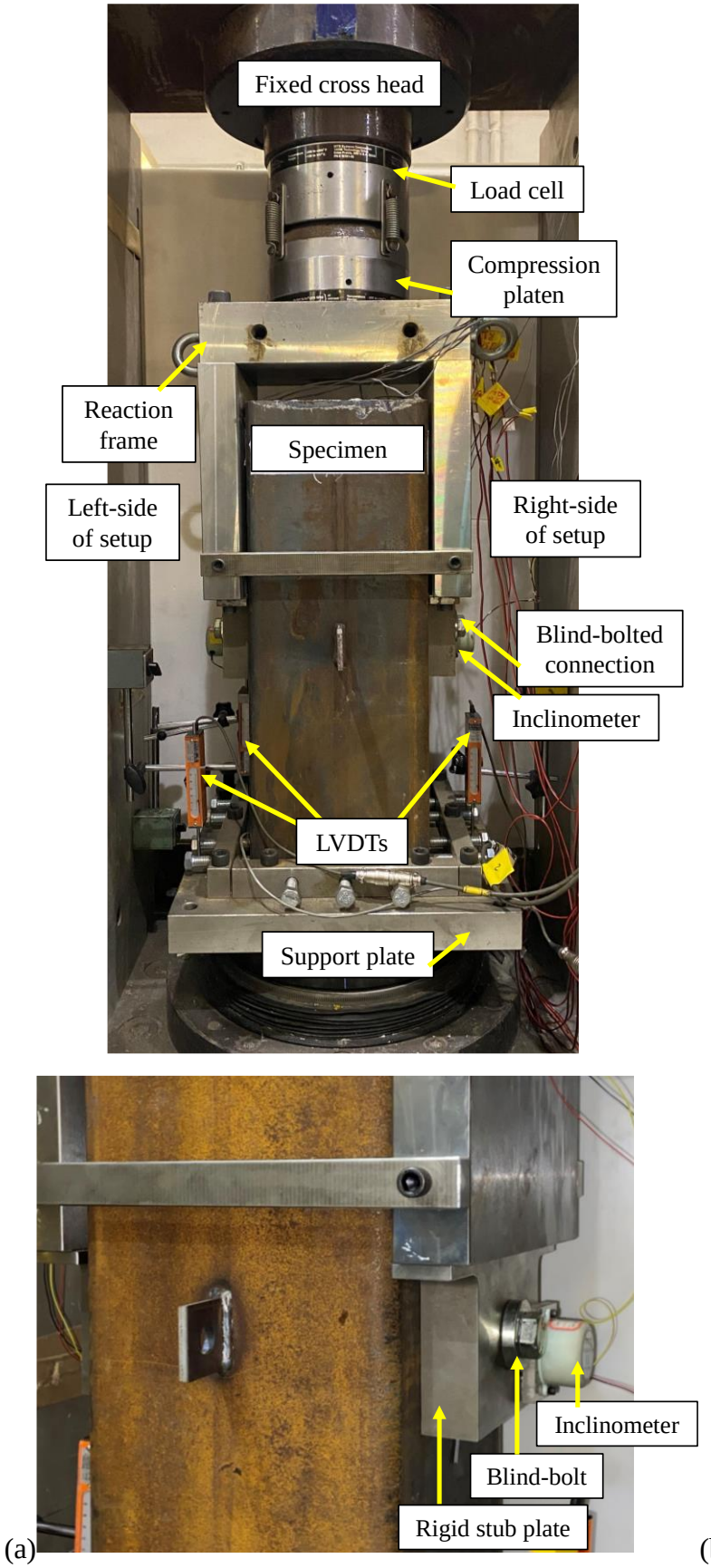

Fig. 5: (a) Actual experimental set up using the MTS 815 Rock Mechanic Testing System; (b) close-up view of the bolted connection region.

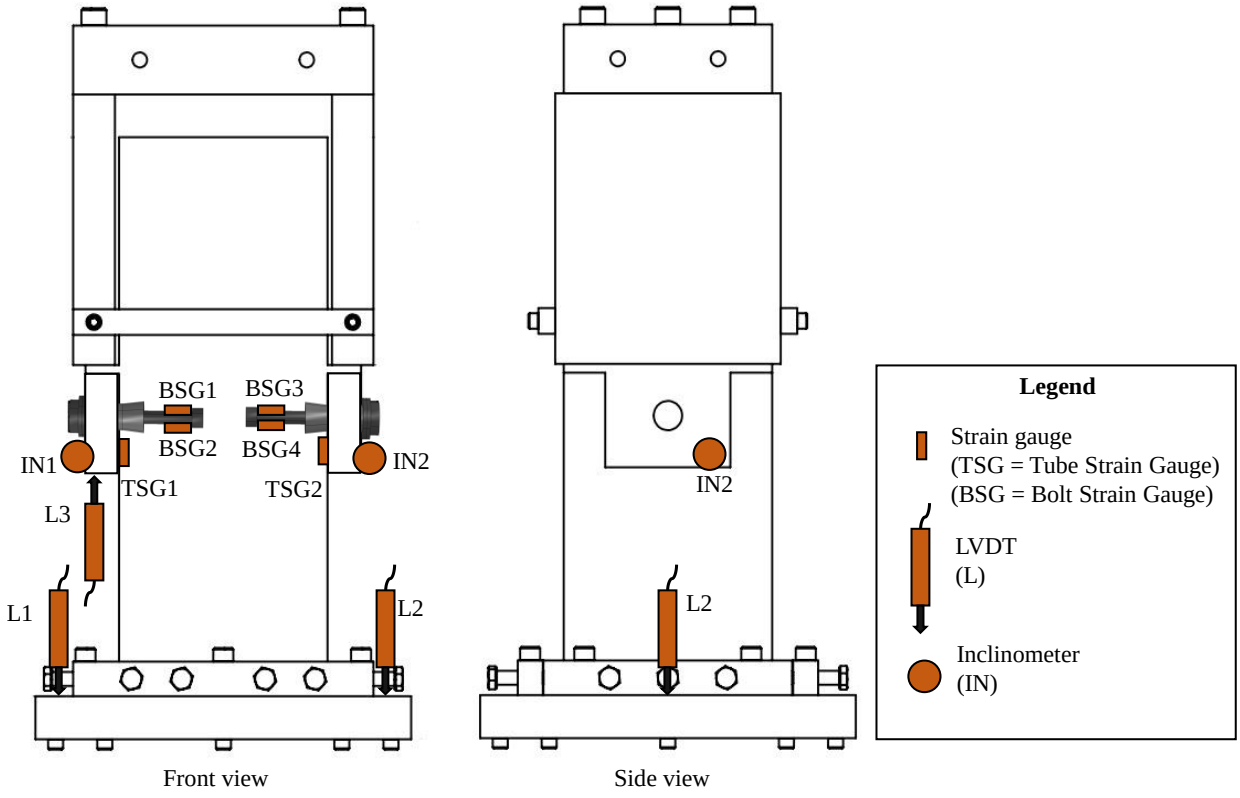

Fig. 6: Positioning of strain gauges, LVDTs and inclinometers.

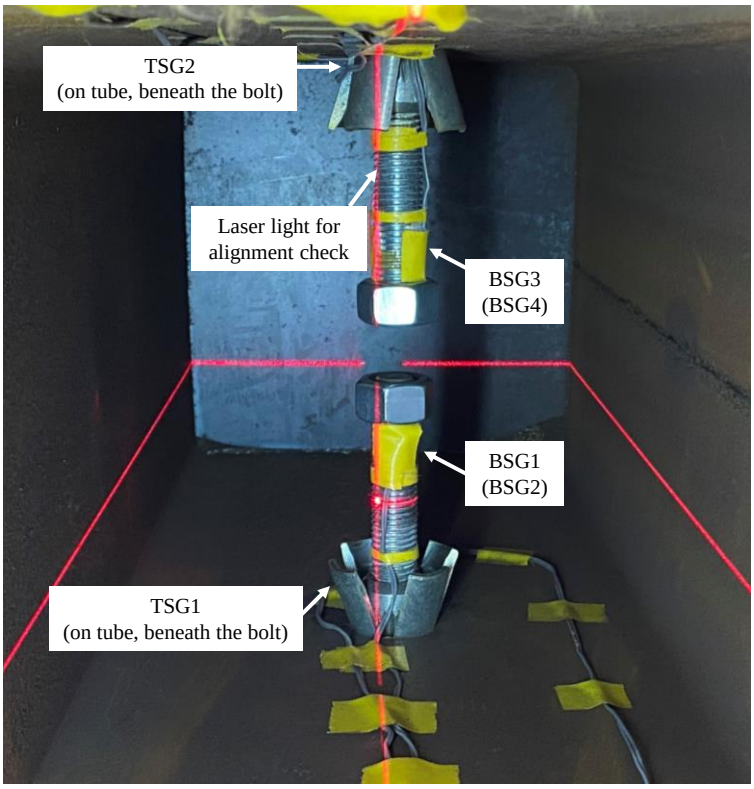

Fig. 7: Inside view of the steel tube attached with strain gauges and check for alignment.

Fig. 8: Tensile testing system for steel tube coupons using Instron UTM.

Fig. 9: Tested (a) tube flat coupons; (b) bolt coupons.

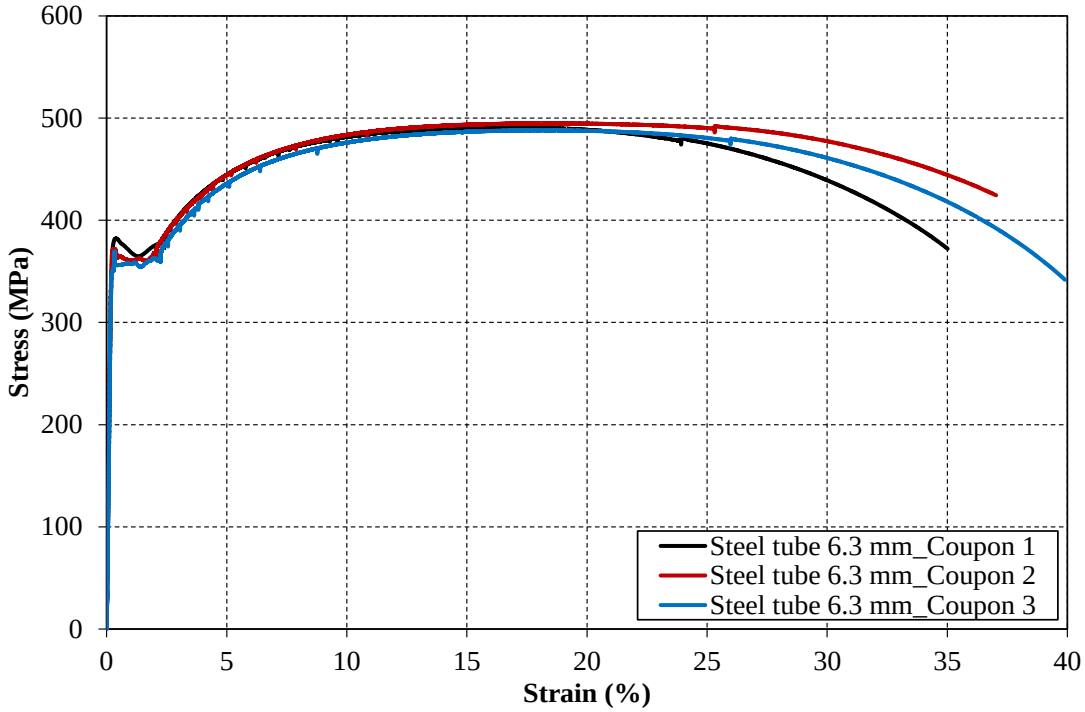

Fig. 10: Stress-strain curve for steel tube with 6.3 mm thickness.

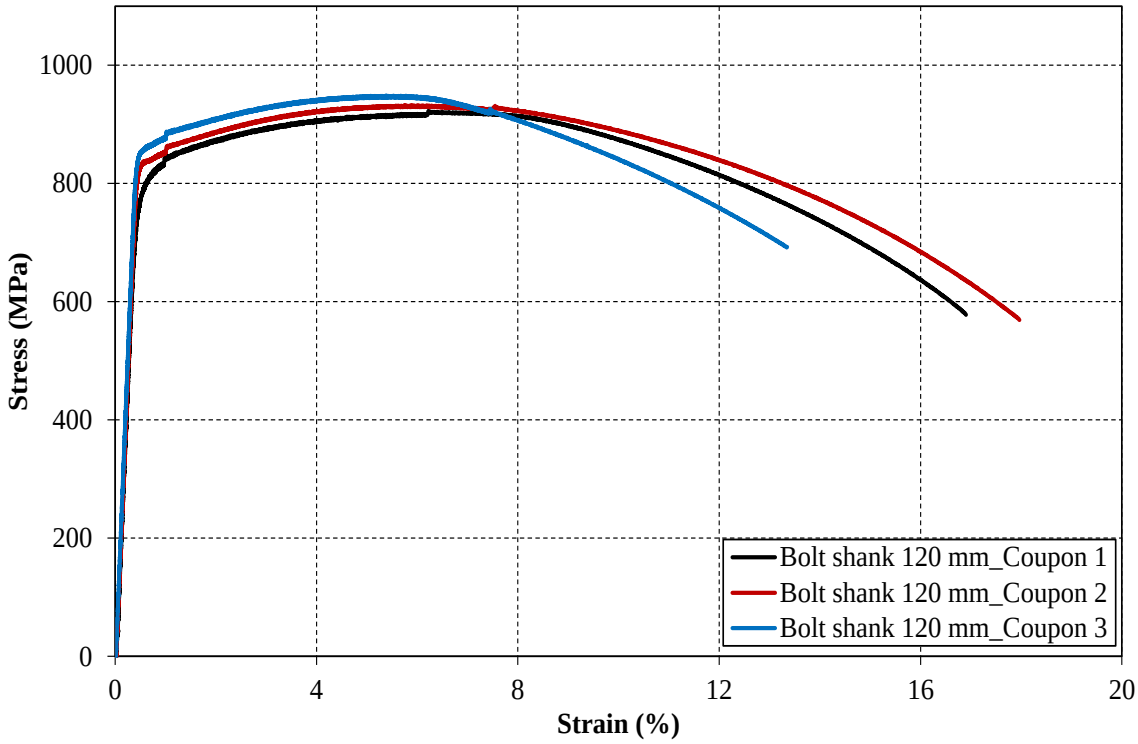

Fig. 11: Stress-strain curve for bolt shank with length 120 mm.

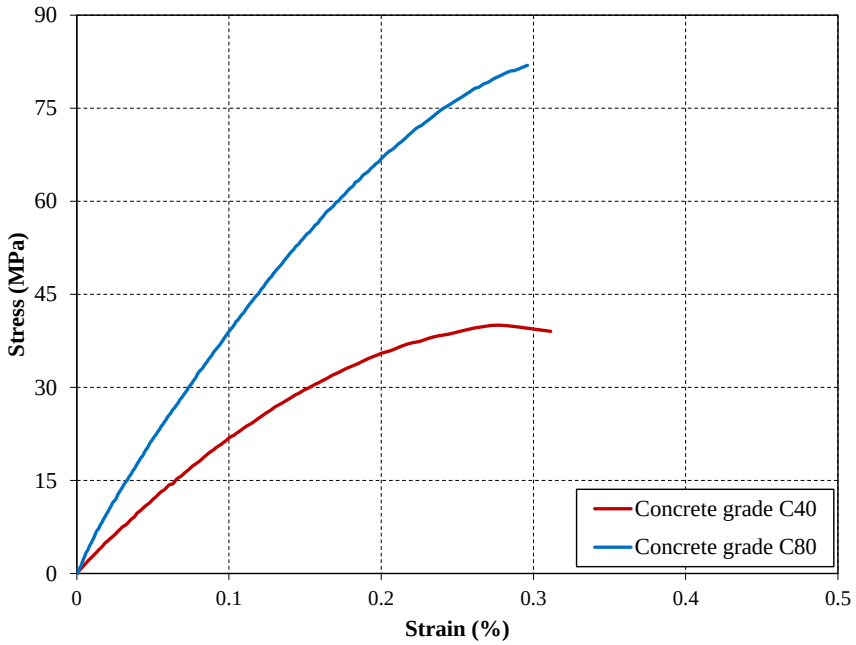

Fig. 12: Stress-strain curve for concrete cylinders.

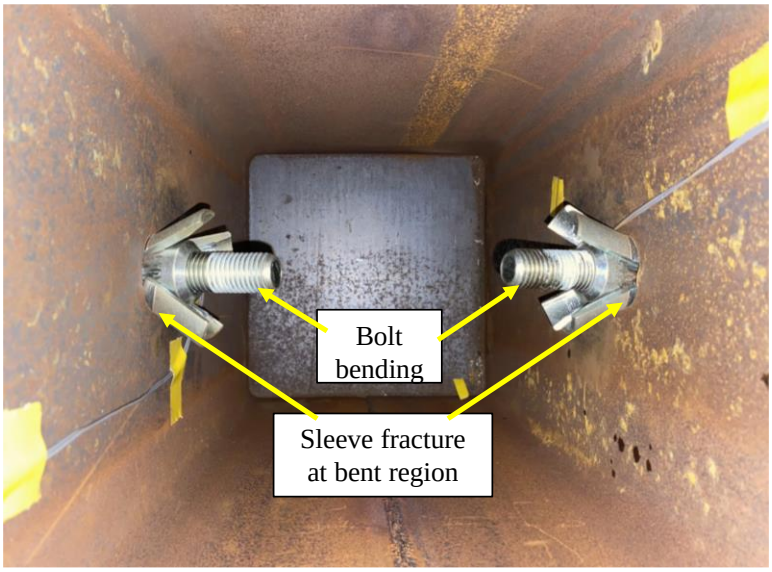

(a)

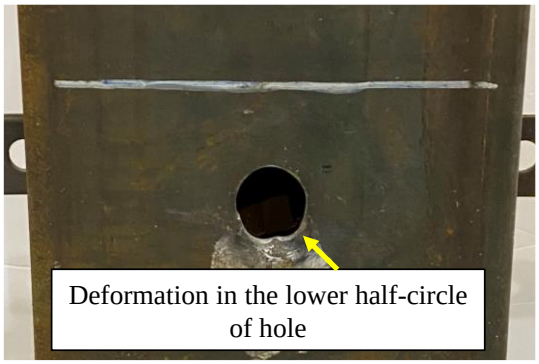

(b)

Fig. 13: Tested specimen A-E65-C0-T6.3; (a) Position of hollo-bolts after test; (b) deformation in tube surface.

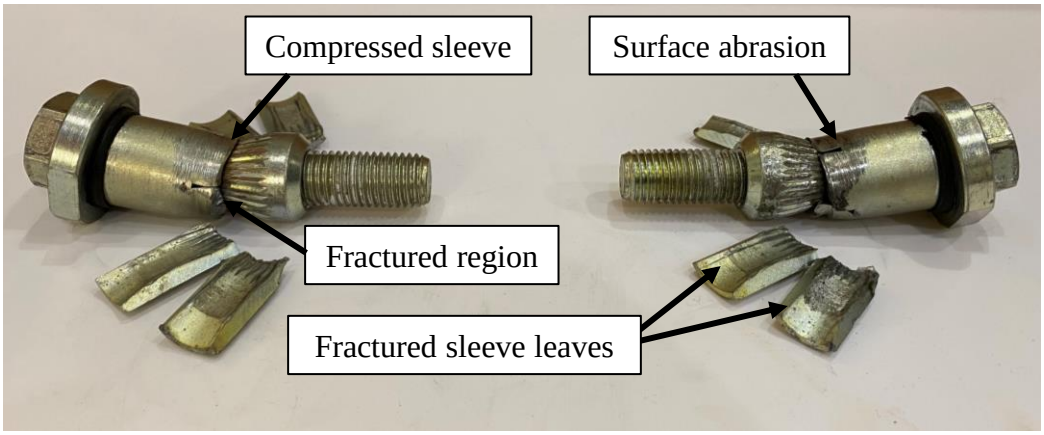

Fig. 14: Hollo-bolts after testing for the specimen A-E65-C0-T6.3.

(a) (b) (c)

Fig. 15: (a) Specimen A-E65-C40-T6.3 after connection failure; (b) Damages in concrete and tube wall; (c) Fractured bolt after test.

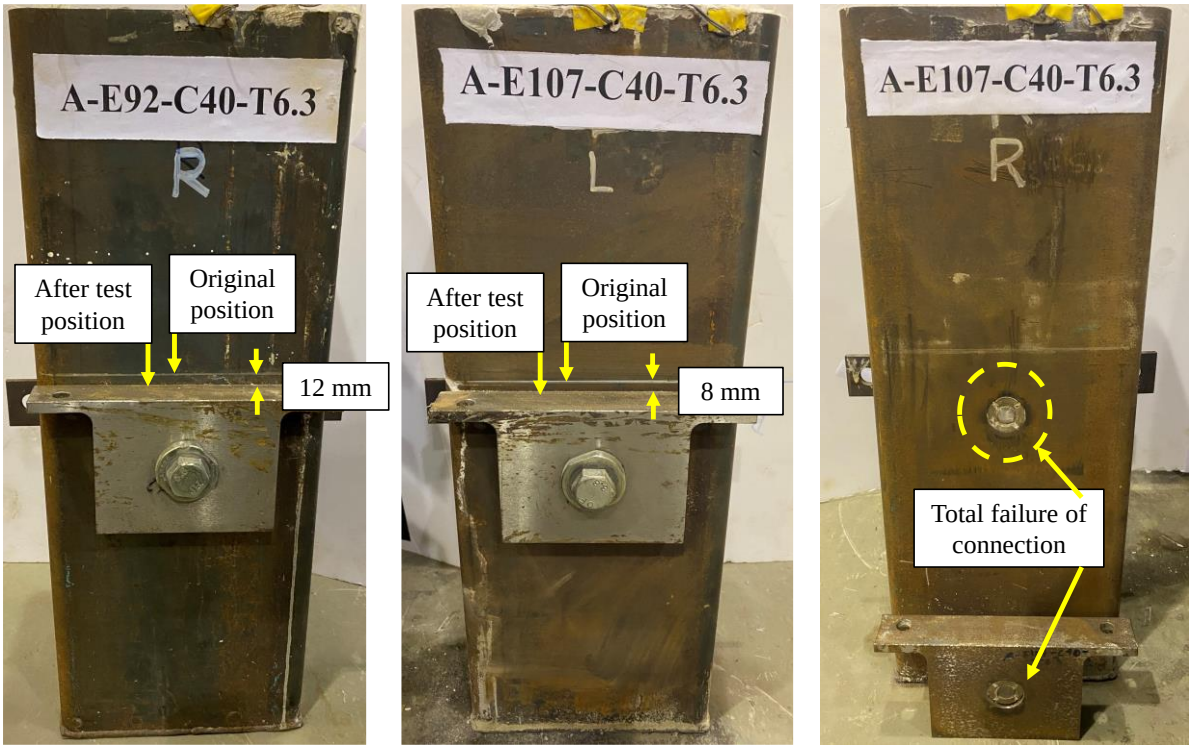

(a) (b) (c)

Fig. 16: (a) Specimen A-E92-C40-T6.3 after testing; (b) left-side of A-E107-C40-T6.3; (c) right-side of A-E107-C40-T6.3.

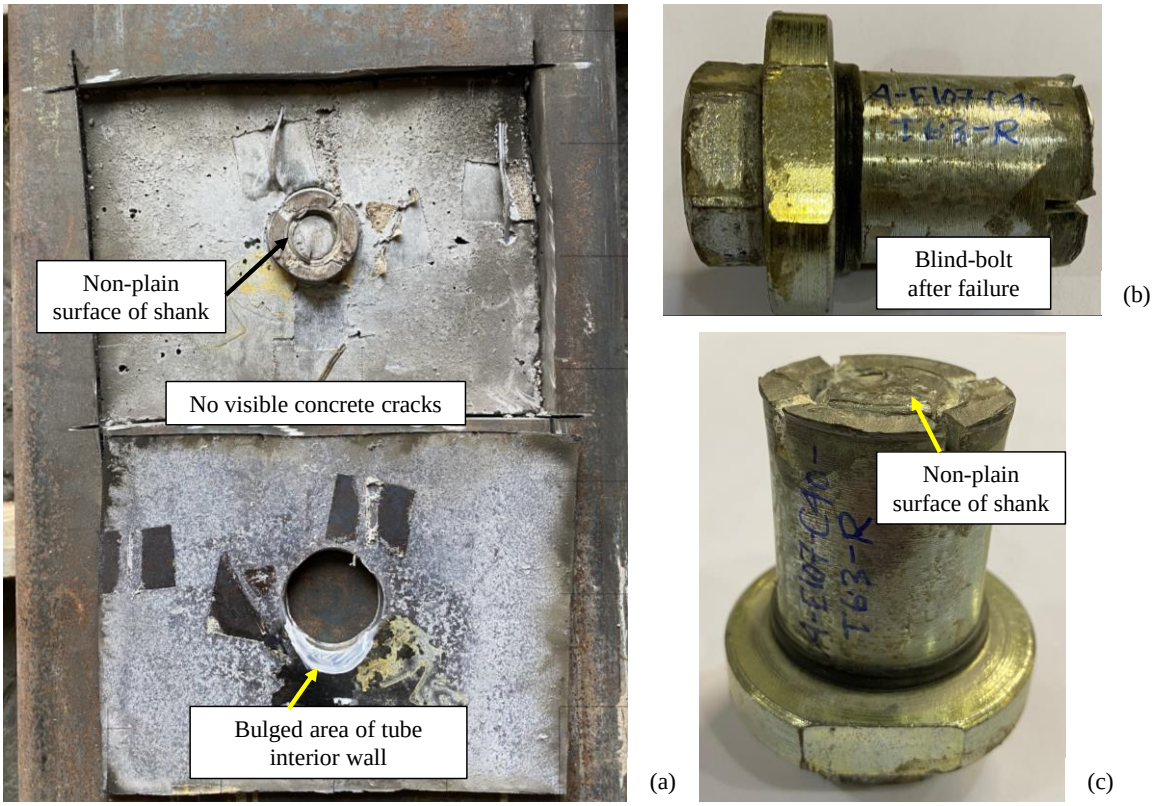

(a) (b) (c)

Fig. 17: Specimen A-E107-C40-T6.3 (a) Concrete and tube wall surface after test; (b) Bolt after shear failure; (c) shank surface after failure.

Fig. 18: Positioning of bolt after shear failure of connection.

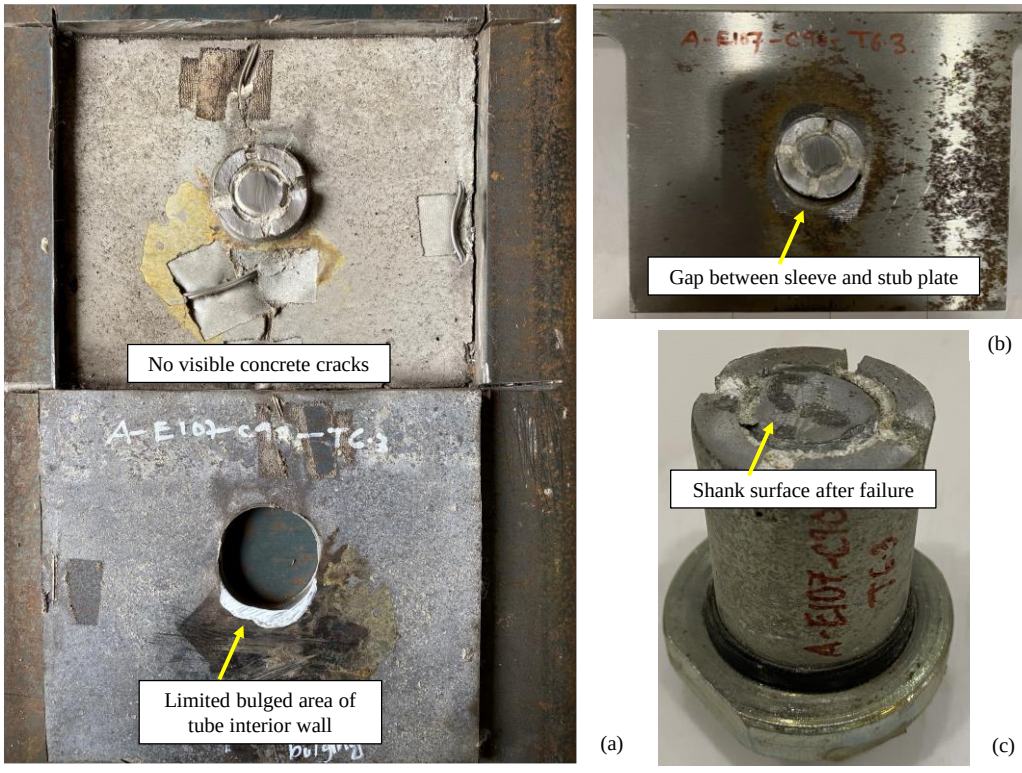

Fig. 19: Specimen A-E107-C80-T6.3 (a) Concrete and tube wall surfaces; (b) bolt part attached to stub plate; (c) shank surface after failure.

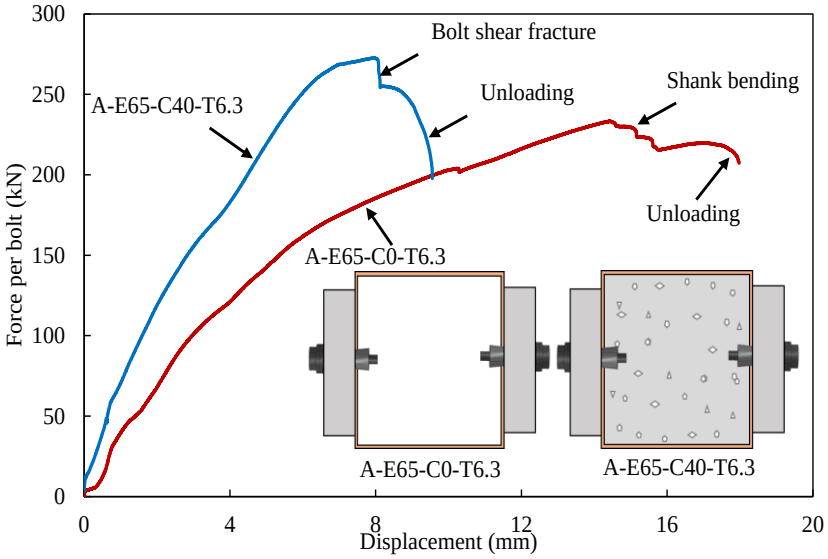

Fig. 20: Influence of concrete infill.

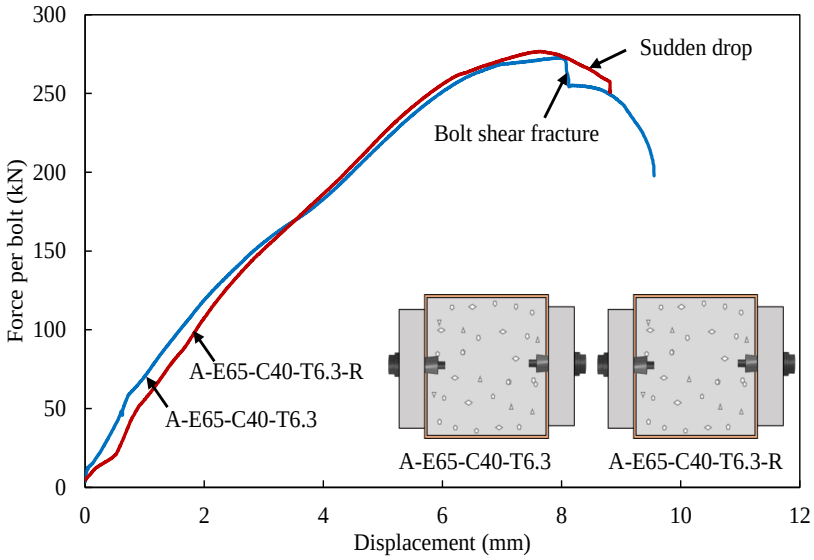

Fig. 21: Comparison between specimens A-E65-C40-T6.3 and A-E65-C40-T6.3-R.

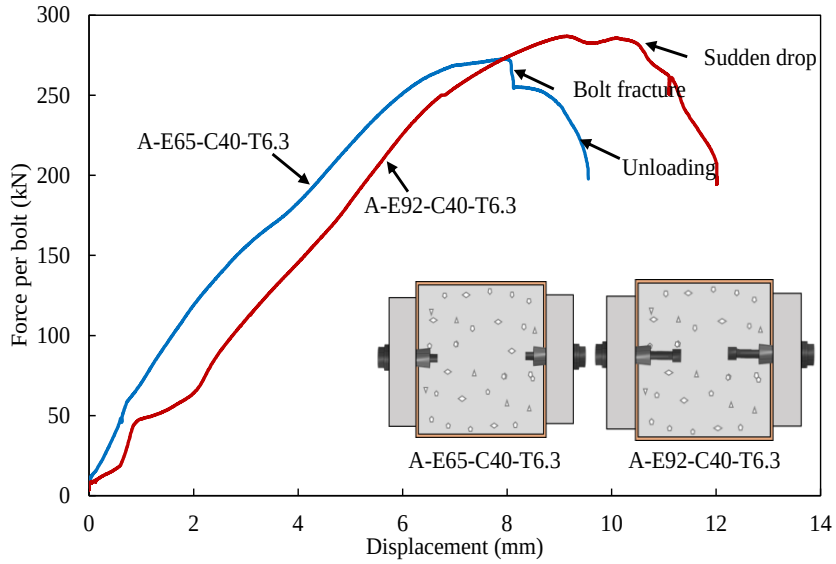

Fig. 22: Comparison between specimens with bolt embedment 3.25d_b and 4.6d_b.

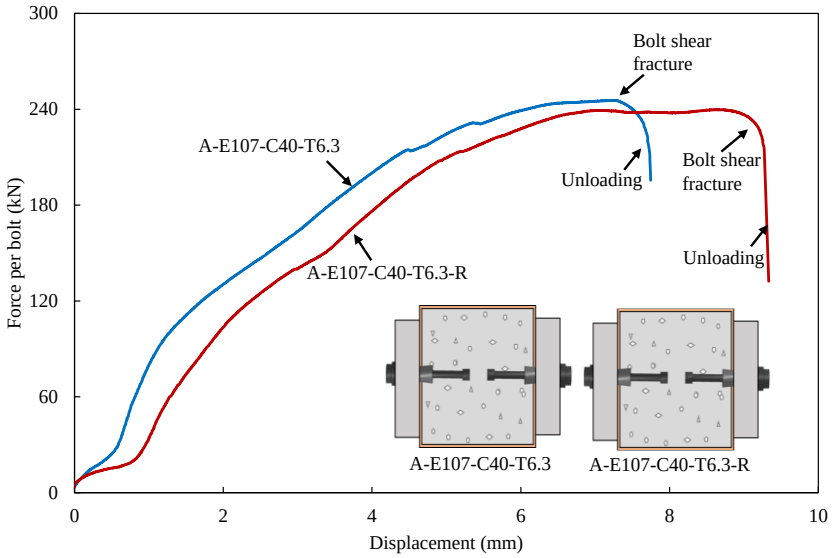

Fig. 23: Comparison between specimens A-E107-C40-T6.3 and A-E107-C40-T6.3-R.

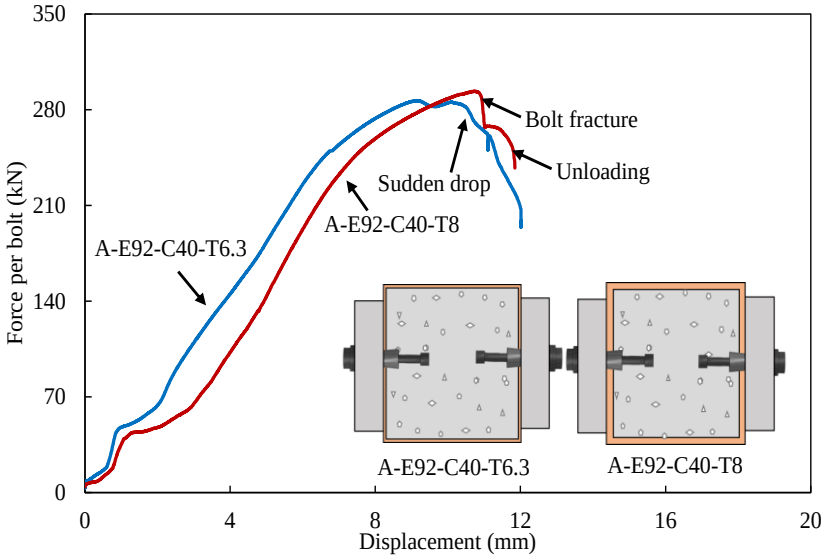

Fig. 24: Influence of tube wall thickness.

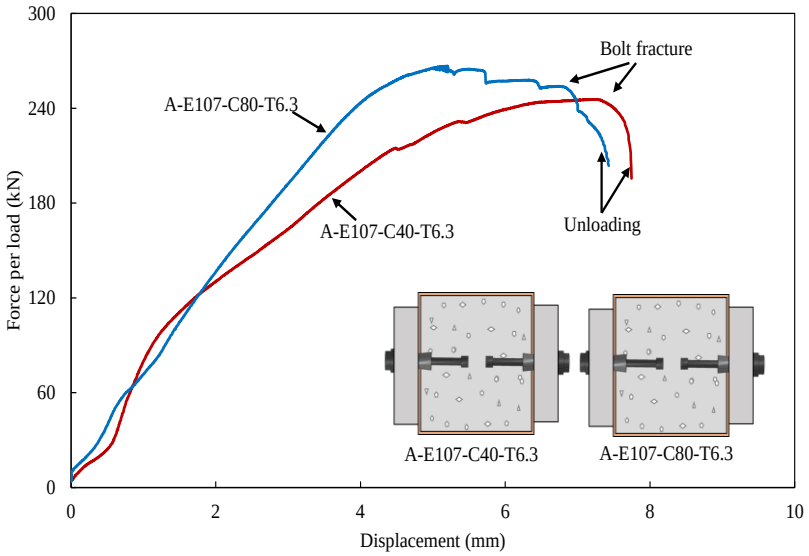

Fig. 25: Influence of infill concrete grade.

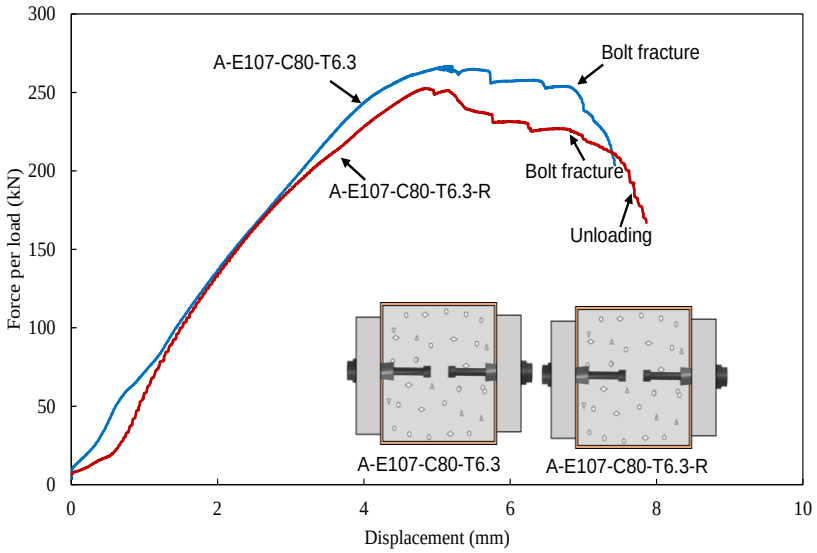

Fig. 26: Comparison between specimens A-E107-C80-T6.3 and A-E107-C80-T6.3-R.

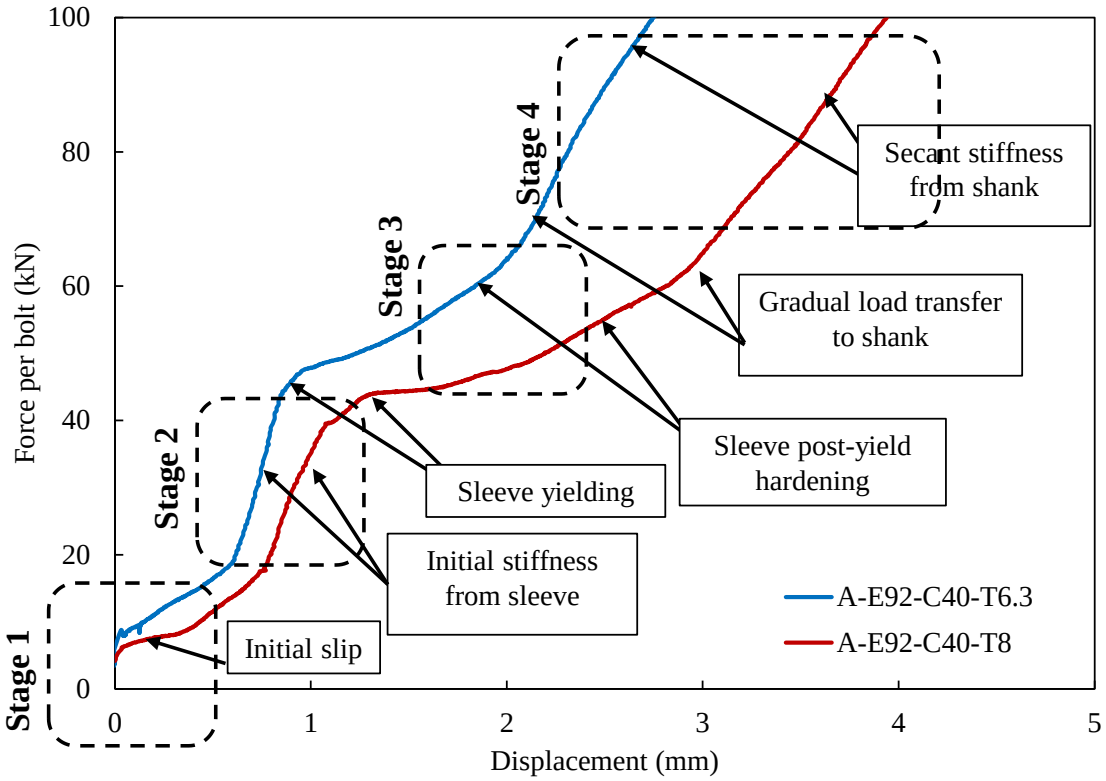

Fig. 27: Load-deformation pattern at the initial stage.

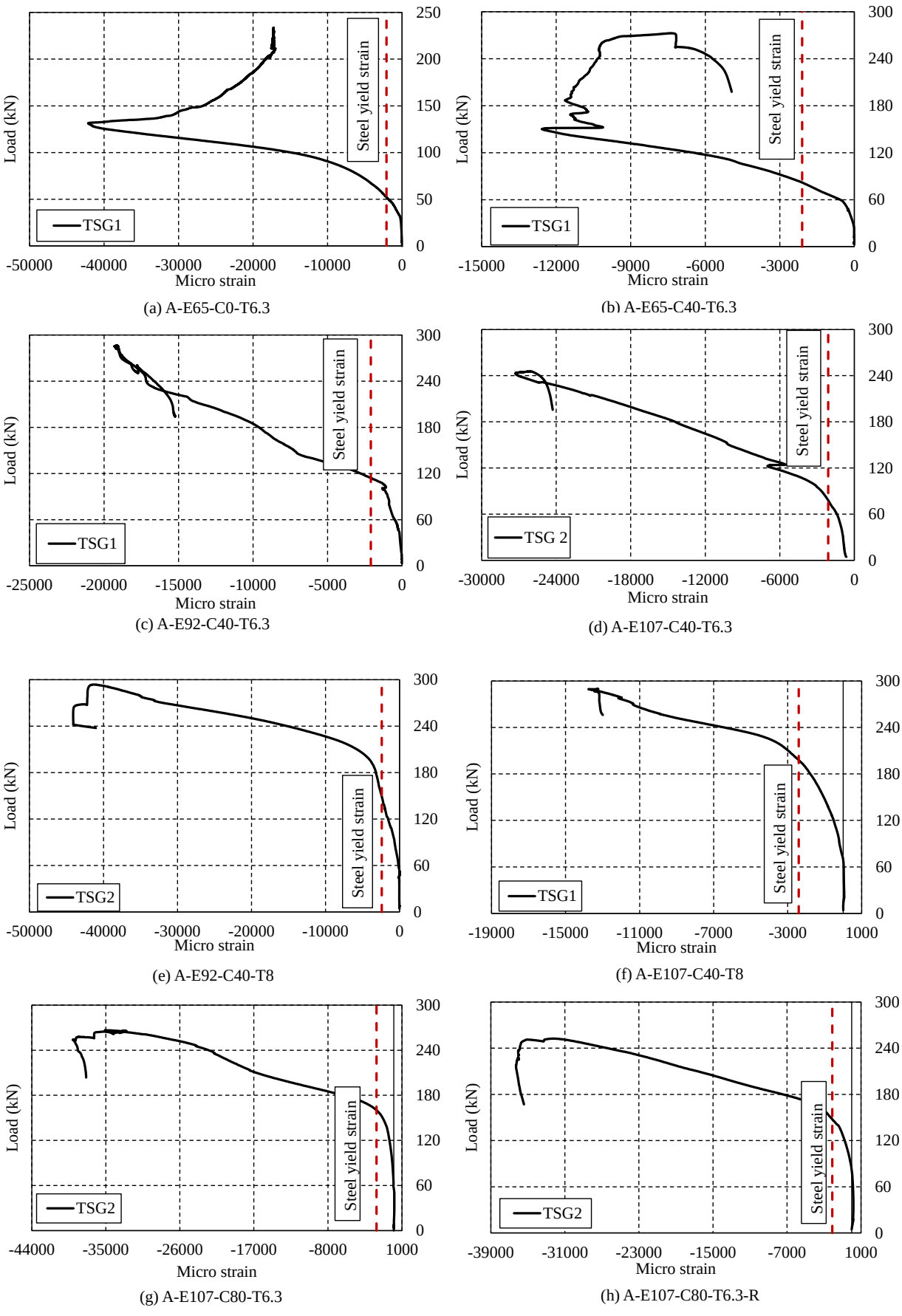

Fig. 28: Strain developed in steel tube below the bolt hole.

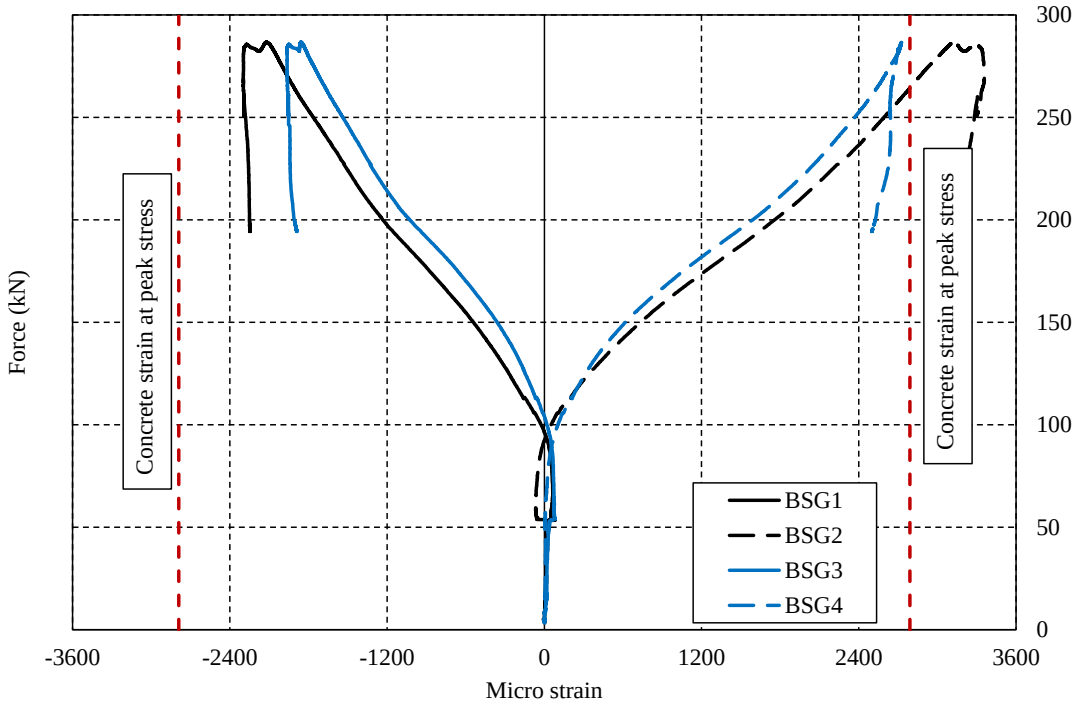

Fig. 29: Strain distribution in concrete core for the specimen A-E92-C40-T6.3.

Table 1: Geometric dimensions of the tested specimens.

Specimen ID	Tube length *(l)* (mm)	Column section *(b × b × t)* (mm)	*b/t*	Corner thickness (mm)	Bolt hole diameter (mm)		Bolt hole location
					Hole 1	Hole 2	
A-E65-C0-T6.3	650	250×249×6.3	39.7	6.46	34.8	34.7	Centre
A-E65-C40-T6.3	650	249×249.5×6.26	39.7	6.66	34.8	34.8	Centre
A-E65-C40-T6.3-R	650	250×250×6.28	39.7	6.5	34.8	34.8	Centre
A-E92-C40-T6.3	650	250×249×6.28	39.7	6.5	35	34.7	Centre
A-E107-C40-T6.3	650	250×249×6.3	39.7	6.46	34.8	35	Centre
A-E107-C40-T6.3-R	650	250×250×6.3	39.7	6.46	35	35	Centre
A-E92-C40-T8	650	249×249.5×8	31.2	8.64	34.8	34.8	Centre
A-E107-C40-T8	650	249×249.5×8	31.2	8.64	34.8	34.8	Centre
A-E107-C80-T6.3	650	249×251×6.28	39.7	6.46	35	35	Centre
A-E107-C80-T6.3-R	650	251×251×6.28	39.7	6.44	34.8	35	Centre

Table 2: Bolt geometric dimensions and other information of specimens.

Specimen ID	Bolt diameter, d_b (mm)		Nominal shear area of shank (A_t) (mm^2)	Net sleeve area (A_{sl}) (mm^2)	Bolt embedment length (mm)	Bolt torque (Nm)	Bolt Property class	Concrete nominal strength (N/mm^2)	Rigid plate thickness (mm)
	Bolt 1	Bolt 2							
A-E65-C0-T6.3	19.8	19.7	245	431.9	65	300	8.8	_	40
A-E65-C40-T6.3	19.8	19.8	245	431.9	65	300	8.8	40	40
A-E65-C40-T6.3-R	19.7	19.8	245	431.9	92	300	8.8	40	40
A-E92-C40-T6.3	19.8	19.8	245	431.9	92	300	8.8	40	40
A-E107-C40-T6.3	19.7	19.7	245	431.9	107	300	8.8	40	40
A-E107-C40-T6.3-R	19.8	19.8	245	431.9	107	300	8.8	40	40
A-E92-C40-T8	19.8	19.8	245	431.9	92	300	8.8	40	40
A-E107-C40-T8	19.8	19.7	245	431.9	107	300	8.8	40	40
A-E107-C80-T6.3	19.7	19.7	245	431.9	107	300	8.8	80	40
A-E107-C80-T6.3-R	19.7	19.7	245	431.9	107	300	8.8	80	40

Table 3: Material properties of steel tubes and blind-bolts.

Steel Material		Coupon	Yield strength, (f_y) (MPa)	Ultimate strength, (f_u) (MPa)	Elastic Modulus, (E_s) (GPa)	f_u/f_y
Steel tube	250 × 250 × 6.3 mm	1	380	491	201.9	1.29
		2	371	494.9	194.5	1.33
		3	368	488	186.7	1.32
	Average		*373*	*491.3*	*194.4*	*1.31*
	250 × 250 × 8 mm	1	342	474	210.6	1.38
		2	357	478.3	192.3	1.34
		3	357	498.1	208	1.40
	Average		*352*	*483.5*	*203.7*	*1.37*
M20 diameter blind-bolt	Shank length 120 mm	1	754	922.57	202.6	1.22
		2	803	932.2	208.8	1.16
		3	824	948.9	213.9	1.15
	Average		*793.6*	*934.5*	*208.4*	*1.17*
	Shank length 150 mm	1	860	972.8	214	1.13
		2	815	965.9	199.2	1.18
		3	842	964.3	204.6	1.14
	Average		*839*	*967.7*	*205.9*	*1.15*
	Shank length 165 mm	1	803	891.6	209.1	1.11
		2	802.1	887.9	209.3	1.10
		3	792.4	883.6	207.5	1.11
	Average		*799.1*	*887.7*	*208.6*	*1.11*
	Sleeve* Batch of shank length 120 mm		396	529	_	1.33
	Batch of shank length 150 mm		390	519	_	1.33
	Batch of shank length 165 mm		393	520	_	1.32

Note: * average sleeve material properties based on hardness test of twelve sleeve leaves from each batch.

Table 4: Mix design and strength properties of concrete.

Concrete grade	Water/ Cement	Water (Kg/m^3)	Cement (Kg/m^3)	Sand (Kg/m^3)	Aggregate (Kg/m^3)		S.P* (Kg/m^3)	Slump (mm)	Cylinder average compressive strength (N/mm^2)	Split tensile strength (N/mm^2)	Elastic modulus E_C (GPa)
					10 mm	20 mm					
C40	0.54	202	370	740	385	610	2.5	125	39.1	3.45	26.5
C80	0.28	140	500	704	422	633	10	120	79.7	6.8	39.6

Note * S.P refers to superplasticizer.

Table 5: Summary of test results and comparison with international codes.

Specimen ID	$F_{v,Exp}$ (kN)	k (kN/mm)	k_{sc} (kN/mm)	$F_{v,EC3}$ (kN)	$F_{v,AISC}$ (kN)	$F_{v,AS}$ (kN)	$F_{v,Prop}$ (kN)	$F_{v,EC8}/F_{v,Exp}$	$F_{vAISC}/F_{v,Exp}$	$F_{v,AS}/F_{v,Exp}$	$F_{v,Prop}/F_{v,Exp}$
A-E65-C0-T6.3	238.5	58.8	55.5	137	128.9	130.3	274.4	0.57	0.54	0.55	1.15
A-E65-C40-T6.3	272.5	105.8	90.2	137	128.9	130.3	274.4	0.50	0.47	0.48	1.00
A-E65-C40-T6.3-R	276.5	101	92	137	128.9	130.3	274.4	0.49	0.46	0.47	0.99
A-E92-C40-T6.3	286.5	73	74.3	142	133	135	276.7	0.49	0.46	0.47	0.96
A-E107-C40-T6.3	245.5	115.4	107	130	121.8	123.2	264.6	0.52	0.49	0.50	1.07
A-E107-C40-T6.3-R	240	89.2	89	130	121.8	123.2	264.6	0.54	0.50	0.51	1.10
A-E92-C40-T8	293.5	54.8	63	142	133.4	135	276.7	0.48	0.45	0.46	0.94
A-E107-C40-T8	289.5	103.5	101	130	121.8	123	264.6	0.44	0.42	0.43	0.91
A-E107-C80-T6.3	266.5	134.7	129	130	121.8	123	264.6	0.48	0.45	0.46	0.99
A-E107-C80-T6.3-R	252.5	131.6	128.3	130	121.8	123	264.6	0.51	0.48	0.49	1.04
							Mean	*0.51*	*0.48*	*0.48*	*1.04*